



HAL
open science

A theoretical model of Leidenfrost's temperature

Sergey Gavrilyuk, Henri Gouin

► **To cite this version:**

Sergey Gavrilyuk, Henri Gouin. A theoretical model of Leidenfrost's temperature. 2022. hal-03617770v1

HAL Id: hal-03617770

<https://hal.science/hal-03617770v1>

Preprint submitted on 23 Mar 2022 (v1), last revised 17 Nov 2022 (v3)

HAL is a multi-disciplinary open access archive for the deposit and dissemination of scientific research documents, whether they are published or not. The documents may come from teaching and research institutions in France or abroad, or from public or private research centers.

L'archive ouverte pluridisciplinaire **HAL**, est destinée au dépôt et à la diffusion de documents scientifiques de niveau recherche, publiés ou non, émanant des établissements d'enseignement et de recherche français ou étrangers, des laboratoires publics ou privés.

A theoretical model of Leidenfrost's temperature

Sergey Gavriluk ^{*} and Henri Gouin [†]

Aix Marseille University, CNRS, IUSTI, UMR 7343, Marseille, France.

Abstract

The *Leidenfrost effect* is a phenomenon in which a liquid, poured onto a surface significantly hotter than the liquid's boiling point, produces a layer of vapor that prevents the liquid from rapid evaporation. Rather than making physical contact, a puddle of water levitates above the surface.

The temperature above which the phenomenon occurs is called *Leidenfrost's temperature*. The reason for the existence of Leidenfrost's temperature, which is much higher than the boiling point of the liquid, is not theoretically understood. Here we prove that Leidenfrost's temperature corresponds to a bifurcation in the solutions of equations describing evaporation of a non-equilibrium liquid–vapor interface. For water, the theoretical values of obtained Leidenfrost's temperature, and that of the liquid bulk which is smaller than the boiling point of liquid, fit the experimental results found in the literature.

Keywords: Leidenfrost effect, non-equilibrium thermodynamics, capillarity effect, dynamic interfaces.

^{*}E-mail: sergey.gavrilyuk@univ-amu.fr

[†]E-Mails: henri.gouin@univ-amu.fr; henri.gouin@yahoo.fr

1 Introduction

When water is projected onto a moderately heated metal plate, it spreads out, starts to boil and evaporates very quickly. Things are quite different when the metal is incandescent: the water temperature remains below the boiling temperature, divides into numerous droplets that roll, and are thrown around without boiling [1, 2, 3, 4, 5, 6]. Observations show that the droplets perform translational and rotational motions. These movements lead to geometrically beautiful patterns. Photographic and stroboscopic tools were then used to describe the experiments, but the effect can be seen with the naked eye. Such a phenomenon is qualitatively very well described in [7, 8]. An analytical model of these figures and movements has been proposed in [9].

This *Leidenfrost effect*, called also *film boiling*, was carefully observed in 1756 by the German physician J. G. Leidenfrost. Leidenfrost had well understood the cause of the film boiling phenomenon: there is no contact between the burning solid and water, the liquid evaporates in the vicinity of the solid and levitates on a cushion of steam [10].

In 1844, M. Boutigny had also experimented on himself some curious facts related to the phenomenon like plunging his hand in a bath of molten iron without burning himself [11]. Fiery coal can reach about 550 degrees Celsius; candidates for walking on hot coals must moisten their feet to benefit from the Leidenfrost effect.

Today, it is no longer these curiosities that are the subject of in-depth studies, but importance of this phenomenon in all industrial sectors where high temperatures are handled [12, 13, 14]. The boiling crisis is often the first step in an explosive process that is generated by the contact of a hot surface and a liquid. If it is well dominated by metallurgists for the hardening of metals, it is not yet the case in other fields where it is the cause of important accidents. For example, in the oil industry, at the bottom of the distillation towers is oil at a temperature of about 400 degrees Celsius. In these towers, very dry steam is injected at the same temperature. When, due to a malfunction in the installation, liquid water is injected, the explosion that occurs is so violent that it destroys most of the distillation plates [15]. In nuclear industry, several accidents were initiated by the phenomenon. In 1961, for the American SL-1 reactor at Idaho State Laboratory, an unexpected lifting of a control bar caused water to be projected over the core onto the vessel which, despite its weight of 13 tons, sheared the pipes to which it was connected and rose about 3 meters. In 1986, the film boiling phenomenon

occurred in Chernobyl, and in 2011 in Fukushima, creating major nuclear accidents. The largest terrestrial explosion ever recorded, that of Krakatoa volcano (in 1883) corresponding to 200 megatons of TNT, is also due to the contact of lava at high temperature with sea water.

These events have given rise to a large number of studies [1, 2, 3, 4, 5, 6, 16, 17, 18]. However, it cannot be said that a satisfactory theory has been developed. Indeed, the Leidenfrost effect still retains an essential mystery about the reason for a temperature above which there is the creation of the vapor film. One may wonder why, under normal atmospheric pressure, the creation of the film does not occur at a temperature close to 100 degrees Celsius, the boiling temperature of water, which creates a large quantity of vapor. Not being the case, the existence of the Leidenfrost temperature has, to our knowledge, never been explained in a satisfactory way.

In order to treat the problem as simply as possible, we consider a thin layer of liquid water on a flat, infinite and horizontal solid surface W . Since the layer is thin, we can neglect the gravitational forces. The liquid water layer is assumed to be separated from a water vapor layer by a liquid–vapor interface. We will assume that the liquid water layer is under atmospheric pressure p_0 , and that the interface and liquid bulk are at the same temperature T_i . The vapor layer between the liquid–vapor interface and the horizontal surface is decomposed into three parts: a very thin upper part in contact with the interface being at the temperature T_i ; a second intermediate part where the temperature varies from T_i to T_w , and finally the last part of the vapor layer at temperature T_w where the vapor is evacuated along the solid surface W . The fluid flows through the liquid–vapor layers perpendicular to W (Figure 1 shows the considered schematization).

Then, we propose a thermo-mechanical model justifying a *bifurcation* temperature below which the existence of the vapor film is impossible and above which the existence of the vapor film is possible. Without pretending that our model will solve all problems posed by the film boiling phenomenon, we think that it can provide an understanding of the phenomenon by explaining the origin of Leidenfrost’s temperature.

To simplify the presentation of the article, we have separate the paper into six sections and three appendices. In Section 2, we present the classical van der Waals equation of state. Section 3 studies the thermo-mechanical van der Waals–Korteweg model across the liquid-vapor interface and in the vapor

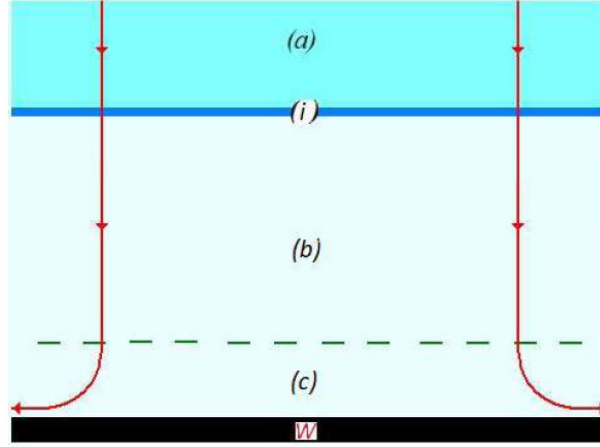


Figure 1: Sketch of a quasi-one-dimensional transverse fluid flow. Domain (a) is a thin liquid layer of temperature T_i ; (i) is the liquid-vapor discontinuity interface which is a very thin region of few nanometers thickness of vapor having the same temperature T_i as in the liquid bulk (a); domain (b) is the non-isothermal part of the vapor flow; the temperature increases from T_i to T_w . Region (c) is the part of the vapor region where the flow is not one-dimensional: the vapor escapes along the solid surface. The arrows represent the flow direction.

part of the flow. Sections 4 and 5 study the dimensionless governing equations of one-dimensional flows. In Section 6 the numerical calculations of the governing equations are performed related to experimental data to obtain the Leidenfrost temperature value. A conclusion ends this presentation. Some technical details are shown in Appendices A, B and C.

2 The van der Waals equation of state

We adapt to our problem the simplest model for the description of equilibrium liquid–vapor interfaces: the van der Waals equation of state. Experimental values of physical quantities at the boiling temperature $T_0 = 373.15^\circ$ Kelvin (corresponding to 100° Celsius) are presented in International System of Units (SI) (see [19]):

$$p_0 \approx 101325 \text{ Pa}, \quad v_g \approx 1.673 \text{ m}^3/\text{kg}, \quad v_l \approx 0.001043 \text{ m}^3/\text{kg},$$

where p_0 is the atmospheric pressure, v_g and v_l are specific volumes of vapor and liquid water at phase equilibrium, respectively. The van der Waals equation of state is:

$$p = \frac{RT}{v-b} - \frac{a}{v^2}, \quad (2.1)$$

where a , b and R are constant. At a given temperature T , one obtains the chemical potential μ (defined up to an additive constant), where $d\mu = v dp$ and $v = 1/\rho$ is the specific volume:

$$\mu(v, T) = -RT \text{Log}(v-b) + \frac{RTb}{v-b} - \frac{2a}{v}. \quad (2.2)$$

The equilibrium Maxwell conditions of liquid-vapor interface are:

$$\begin{cases} \frac{RT_0}{v_g-b} - \frac{a}{v_g^2} = \frac{RT_0}{v_l-b} - \frac{a}{v_l^2} = p_0, \\ \mu(v_g, T_0) = \mu(v_l, T_0). \end{cases} \quad (2.3)$$

At $T_0 = 373.15^\circ$ Kelvin, we obtain:

$$a \approx 1.52 \times 10^3 \text{ m}^5 \text{ s}^{-2}, \quad b \approx 9.2 \times 10^{-4} \text{ m}^3 \text{ kg}^{-1}, \quad R \approx 456 \text{ m}^2 \text{ s}^{-2} \text{ K}^{-1}. \quad (2.4)$$

When v is large, the van der Waals equation (2.1) yields the equation of state of perfect gas $pv = RT$ where R is the ideal gas constant at 100° Celsius. We define a characteristic specific volume v_0 of the vapor phase as:

$$p_0 v_0 = RT_0,$$

which gives:

$$v_0 \approx 1.68 \text{ m}^3 \text{ kg}^{-1}.$$

Van der Waals' model is a qualitatively realistic equilibrium model even far from the boiling point. Indeed, when we consider vapor and liquid water near 160° Celsius, we obtain from system (2.3) other values of coefficients a , b and R :

$$a \approx 1.40 \times 10^3 \text{ m}^5 \text{ s}^{-2}, \quad b \approx 9.3 \times 10^{-4} \text{ m}^3 \text{ kg}^{-1}, \quad R \approx 447 \text{ m}^2 \text{ s}^{-2} \text{ K}^{-1}. \quad (2.5)$$

Even the values of a , b vary with the temperature, their effect on the pressure variation is smaller than 0.5%. The variation of R gives an error in the pressure value smaller than 2%.

3 A continuous theory of capillarity

The second gradient theory [20], conceptually more straightforward than the Laplace theory, can be used to construct a continuous theory for fluid interfaces [21]. Rowlinson and Widom wrote in [22]: *the view that the interfacial region may be treated as matter in bulk, with a local free-energy density that is that of hypothetically uniform fluid of composition equal to the local composition, with an additional term arising from the non-uniformity, and that the latter may be approximated by a gradient expansion typically truncated in second order, is then most likely to be successful and perhaps even quantitatively accurate.* The essential difference compared to classical compressible fluids is that the specific internal energy depends not only on the density $\rho = 1/v$, specific entropy η , but also of $\nabla\rho$. The specific internal energy α characterizes both the compressibility and capillarity properties of the fluid. Due to fluid isotropy, this energy depends only on the norm of density gradient. The simplest expression of the specific energy is [22]:

$$\alpha = \varepsilon(\rho, \eta) + \frac{\lambda}{2\rho} |\nabla\rho|^2, \quad \lambda = \text{const.} \quad (3.6)$$

Here $\varepsilon(\rho, \eta)$ is the classical specific energy and λ is a capillary coefficient. Such a gradient density dependent energy appears not only in the vicinity of the thermodynamic critical point, but also in the case of large velocity fluctuations. This is the case for vapor created by the boiling of a film [6].

3.1 Conservative motions

For conservative motions, the van der Waals–Korteweg equations of non-homogeneous capillary fluids can be derived from the *Hamilton principle of stationary action* by using the well-known Lagrangian [23, 24, 25, 26]:

$$\mathcal{L} = \rho \left(\frac{|\mathbf{u}|^2}{2} - \alpha - \Omega \right),$$

where \mathbf{u} is the velocity, Ω is the specific potential of external forces, and α is given by (3.6). The usual constraints are the mass and entropy conservation laws:

$$\frac{\partial\rho}{\partial t} + \text{div}(\rho\mathbf{u}) = 0, \quad (3.7)$$

and

$$\frac{\partial \rho \eta}{\partial t} + \operatorname{div}(\rho \eta \mathbf{u}) = 0. \quad (3.8)$$

We refer to calculations in [20, 21, 27] to directly write the governing equations in the form:

$$\frac{\partial \rho \mathbf{u}}{\partial t} + \operatorname{div}(\rho \mathbf{u} \otimes \mathbf{u} - \boldsymbol{\sigma}) + \rho \nabla \Omega = \mathbf{0}, \quad (3.9)$$

where

$$\boldsymbol{\sigma} = - \left(p - \frac{\lambda}{2} |\nabla \rho|^2 - \lambda \rho \Delta \rho \right) \mathbf{I} - \lambda \nabla \rho \otimes \nabla \rho, \quad p = \rho^2 \frac{\partial \varepsilon(\rho, \eta)}{\partial \rho}.$$

Due to a small thickness of a fluid layer, gravitational forces will be neglected. As a consequence of (3.7), (3.8) and (3.9), one obtains the energy equation :

$$\frac{\partial e}{\partial t} + \operatorname{div} \left(e \mathbf{u} - \boldsymbol{\sigma} \mathbf{u} - \lambda \frac{d\rho}{dt} \nabla \rho \right) = 0, \quad e = \rho \left(\frac{|\mathbf{u}|^2}{2} + \alpha \right). \quad (3.10)$$

In the one-dimensional case, the x -axis is drawn perpendicular to the heated surface (see Figure 1). The governing equation (3.9) is written as:

$$\frac{\partial}{\partial t}(\rho u) + \frac{\partial}{\partial x}(\rho u^2 + P) = 0, \quad (3.11)$$

where

$$P = p + k, \quad \text{and} \quad k = \frac{\lambda}{2} \left(\frac{\partial \rho}{\partial x} \right)^2 - \lambda \rho \frac{\partial^2 \rho}{\partial x^2}. \quad (3.12)$$

Here t denotes the time, x the space variable orthogonal to the solid surface, u is the corresponding scalar velocity. At a given temperature T , Eq. (3.11) admits the conservation law:

$$\frac{\partial u}{\partial t} + \frac{\partial}{\partial x} \left(\frac{u^2}{2} + \mu(\rho, T) - \lambda \frac{\partial^2 \rho}{\partial x^2} \right) = 0, \quad (3.13)$$

associated with chemical potential μ (a particular case (2.2) of μ is calculated for the van der Waals equation of state).

Depending on other additional constraints (isothermal or isobaric processes), we consider the chemical potential or the specific enthalpy instead of the specific internal energy (the details are further explained).

3.2 One-dimensional stationary vapor motions

In rest of the paper, the liquid thin layer is assumed to be fed by an auxiliary device that allows the motion to be steady. We consider domains (*a*), (*b*), (*c*) and interface (*i*) separating domains of liquid (*a*) and vapor (*b*) (Figure 1).

In the one-dimensional stationary case, Eq. (3.7) yields:

$$\rho u = q, \quad q = \text{const}, \quad (3.14)$$

where q represents the constant flow rate of the fluid.

Equation (3.11) writes:

$$\frac{d}{dx} (\rho u^2 + P) = 0, \quad (3.15)$$

• Through the liquid–vapor interface, Eq. (3.11) implies the jump condition:

$$[P + q^2 v] = 0,$$

i.e.

$$P_i - p_0 + q^2(v_{g_i} - v_{l_i}) = 0, \quad (3.16)$$

where we denote by $v_{l_i} = 1/\rho_{l_i}$ ($v_{g_i} = 1/\rho_{g_i}$) the liquid (vapor) specific volume at interface (*i*), and the square brackets mean the difference of values across interface (*i*). Since the liquid layer is thin, the gravity is not taken into account, thus the pressure is atmospheric pressure p_0 in the liquid bulk.

• In domains (*b*), we obtain from (3.15):

$$P_i - p_w + q^2(v_{g_i} - v_w) = 0,$$

The vapor on the boundary between (*b*) and in domain (*c*) is assumed to be at temperature T_w and homogeneous; p_w is its corresponding pressure and v_w is its specific volume. The difference with Eq. (3.16) yields:

$$p_w - p_0 + q^2(v_w - v_{l_i}) = 0. \quad (3.17)$$

- The motion in the bulk (*a*) and the jump through the interface is assumed to be isothermal. Consequently, we have to use the conservation law (3.13). The corresponding jump relation is:

$$\left[\frac{u^2}{2} + \mu(\rho, T_i) - \lambda \frac{d^2 \rho}{dx^2} \right] = 0, \quad (3.18)$$

where $\mu(\rho, T_i)$ is defined by (2.2). Equation (3.18) can be considered as a dynamical Maxwell rule (see also Appendix (B.1)).

- The vapor motion in domain (*b*) is not isothermal. The viscosity of the vapor phase is negligible, so the equation of motion (3.15) is unchanged. The equation of the energy balance (3.10) in the vapor phase must take account of the heat exchange in the vapor region. Such a balance equation is in the form:

$$\left\{ (e + P) u - \lambda \left(\frac{d\rho}{dx} \right)^2 u \right\}_{|\rho_{g_i}, T_i} - \left\{ (e + P) u - \lambda \left(\frac{d\rho}{dx} \right)^2 u \right\}_{|\rho_w, T_w} = \dot{Q}_w - \dot{Q}_i. \quad (3.19)$$

Compared to (3.10), we added in the total energy the balance of heat fluxes $\dot{Q}_w - \dot{Q}_i$. Also, since the flow volume is fixed, it changes the expression of e (for proof, see Appendix B.2):

$$e = \rho(u^2/2 + H) \quad \text{with} \quad H = \alpha + \frac{p_0}{\rho} = \varepsilon + \frac{\lambda}{2\rho} \left(\frac{d\rho}{dx} \right)^2 + \frac{p_0}{\rho}.$$

The expression of P is given by (3.12). In the domain (*c*) near the surface W the density becomes homogeneous and the balance law (3.19) becomes:

$$\left\{ (e + P) u - \lambda \left(\frac{d\rho}{dx} \right)^2 u \right\}_{|\rho_{g_i}, T_i} - \{(e + P) u\}_{|\rho_w, T_w} = \dot{Q}_w - \dot{Q}_i. \quad (3.20)$$

The vapor density strongly varies near and through the interface.

At the interface, considered as a discontinuity, an extra condition must be added on both sides of the interfacial discontinuity:

$$\frac{d\rho}{dx} = 0. \quad (3.21)$$

This additional condition (3.21) is fundamental in the rest of our paper. It is recalled and explained in Appendix A. Also, condition (3.21) is obtained and analyzed in [25, 28, 29]. Physically, it means the absence of microenergy concentration at the surface of discontinuity. Such a condition also appears when a capillary fluid is in contact with a surface when the surface is neither attractive or repulsive [30, 31, 32].

The density jump implies $d^2\rho/dx^2 < 0$, and consequently, due to (3.12), $k > 0$ (this property is analyzed in Fig. 8 (left diagram) of Appendix C).

The vapor at temperature T_w is assumed homogeneous. Using the relation (3.20) complemented by (3.21), we get:

$$\frac{1}{2} \frac{q^3}{\rho_i^2} + p_i v_{g_i} q - \lambda \frac{d^2 \rho_{g_i}}{dx^2} q + H_i q + \dot{Q}_i = \frac{1}{2} \frac{q^3}{\rho_w^2} + p_w v_w q + H_w q + \dot{Q}_w,$$

with $H = \varepsilon + p_0 v$. Here indices “ i ” and “ w ” mean values of variables at the interface and surface, respectively. In the above relation the second derivative of the density ρ_{g_i} is - *à priori* - non-vanishing.

The heat flux can be written $\dot{Q} = \Lambda q$ where Λ is an associated heat per unit mass.

Since $k = -\lambda \rho_{g_i} \frac{d\rho_{g_i}^2}{dx^2}$ and $P_i = p_i + k$, we get:

$$\frac{1}{2} q^2 v_{g_i}^2 + H_i + P_i v_{g_i} + \Lambda_i = \frac{1}{2} q^2 v_w^2 + H_w + p_w v_w + \Lambda_w. \quad (3.22)$$

Let us underline that:

$$p_i = p(v_{g_i}, T_i), \quad p_w = p(v_w, T_w).$$

From Eq. (2.1), we have [33]:

$$\varepsilon = \int c_v(T) dT - \frac{a}{v},$$

where $c_v(T)$ is the specific heat of water vapor at constant volume. Equation (3.22) implies:

$$\begin{aligned} & \frac{1}{2} q^2 (v_{g_i}^2 - v_w^2) + \int_{T_w}^{T_i} c_v(T) dT + 2k v_{g_i} + \\ & 2 \left(\frac{RT_i v_{g_i}}{v_{g_i} - b} - \frac{RT_w v_w}{v_w - b} \right) - \frac{a}{v_{g_i}} + \frac{a}{v_w} + \Lambda_i - \Lambda_w = 0. \end{aligned} \quad (3.23)$$

We approximate the vapor equation of state by $p_i v_{g_i} \approx RT_i$, $p_w v_w \approx RT_w$, and introduce

$$c_p(T) = c_v(T) + R,$$

corresponding to the specific heat at constant pressure which depends only on temperature T . We obtain from (3.23):

$$\frac{1}{2} q^2 (v_{g_i}^2 - v_w^2) + \int_{T_w}^{T_i} c_p(T) dT + 2k v_{g_i} + R(T_i - T_w) + \Lambda_i - \Lambda_w = 0, \quad (3.24)$$

To transform a liquid into saturated vapor, we need to supply latent heat L . At a given temperature, and for the van der Waals equation of state, the energy of a saturated vapor is approximately independent on the pressure. Indeed, for a given temperature T , the energy variation is:

$$\varepsilon(v_g, T) - \varepsilon(v_{g_s}, T) = a \left(\frac{1}{v_{sg}} - \frac{1}{v_g} \right) \approx 0,$$

where v_{sg} is the specific volume of saturated vapor at pressure p_s (index s means saturated), and v_g is the specific volume of vapor at pressure p_0 . Compared to the latent heat value, this variation is small even for large variation of the specific volume of the vapor.

Since $L = \varepsilon + p v$, one has:

$$L_i - L_w = (\varepsilon(v_{sg_i}, T_i) + p_{si} v_{sg_i}) - (\varepsilon(v_{sg_w}, T_w) + p_{sw} v_{sg_w}).$$

The saturated vapor equation of state being approximated as a perfect gas :

$$p_{si} v_{sg_i} \approx RT_i, \quad \text{and} \quad p_{sw} v_{sg_w} \approx RT_w.$$

Hence,

$$L_i - L_w \approx \varepsilon(v_{sg_i}, T_i) - \varepsilon(v_{sg_w}, T_w) + R(T_i - T_w).$$

At atmospheric pressure, the water vapor equation of state can also be approximated as a perfect gas:

$$p_0 v_{g_i} \approx RT_i, \quad \text{and} \quad p_0 v_{g_w} \approx RT_w,$$

and as in [6], we assume that:

$$\Lambda_i - \Lambda_w \approx L(T_i) - L(T_w).$$

Thus, Eq. (3.24) yields:

$$\frac{1}{2} q^2 (v_{g_i}^2 - v_w^2) + \int_{T_w}^{T_i} c_p(T) dT + 2k v_{g_i} + R(T_i - T_w) + L(T_i) - L(T_w) = 0, \quad (3.25)$$

4 Dimensionless equations of motion

We now consider the dimensionless form of the governing equations. The dimensionless variables are denoted by the same letters but with an additive *tilde sign*. In particular, van der Waals equation of state (2.1) in dimensionless form is:

$$\tilde{p} = \frac{\tilde{T}}{\tilde{v} - \tilde{b}} - \frac{\tilde{a}}{\tilde{v}^2}. \quad (4.26)$$

with

$$\tilde{a} = \frac{a}{p_0 v_0^2}, \quad \tilde{b} = \frac{b}{v_0}, \quad \tilde{T} = \frac{T}{T_0}, \quad \tilde{p} = \frac{p}{p_0}, \quad \tilde{v} = \frac{v}{v_0}, \quad (4.27)$$

where p_0, T_0 are defined in Section 2 and v_0 is defined from $p_0 v_0 = R T_0$. We also introduce the dimensionless variables associated with capillary pressure term, specific volumes and flow rate:

$$\tilde{P}_i = \frac{P_i}{p_0}, \quad \tilde{k} = \frac{k}{p_0}, \quad \tilde{v}_{g_i} = \frac{v_{g_i}}{v_0}, \quad \tilde{v}_{l_i} = \frac{v_{l_i}}{v_0}, \quad \tilde{q} = \frac{q}{q_0} \quad \text{with} \quad q_0 = \sqrt{\frac{p_0}{v_0}}.$$

The equation (3.16) takes the following form:

$$\tilde{P}_i - 1 + \tilde{q}^2 (\tilde{v}_{g_i} - \tilde{v}_{l_i}) = 0,$$

The dimensionless flow rate \tilde{q} is very small. Indeed, when the solid surface temperature is close to the Leidenfrost temperature, the lifetime of liquid dramatically increases, typically by a factor of 500 associated with the existence of a vapor layer isolating the liquid bulk. For example, a millimeter liquid layer on a duralumin surface at 200° Celsius is observed to float for more than a whole minute [6, 34]. So, the fluid velocity due to the liquid evaporation is about $1.7 \times 10^{-5} \text{ m s}^{-1}$, and the flow rate $q \approx 1.7 \times 10^{-2} \text{ kg m s}^{-1}$. For $q_0 = \sqrt{\frac{p_0}{v_0}} \approx 245 \text{ kg m s}^{-1}$, one has $\tilde{q} \approx 7 \times 10^{-5} \ll 1$. Consequently, we can neglect \tilde{q}^2 in the dimensionless governing equations.

The water vapor at pressure p_0 can be considered as a perfect gas and we obtain from Eqs. (3.16)–(3.17):

$$p_w \approx P_i \approx p_0, \quad p_0 v_w \approx R T_w.$$

In dimensionless form we get:

$$\tilde{v}_w \approx \tilde{T}_w \quad \text{and} \quad \tilde{P}_i \approx \tilde{p}_w \approx 1.$$

The pressure in vapor at temperature T_w is also the atmospheric pressure p_0 .

From $p_i v_{g_i} = R T_i$, we obtain as a consequence of motion equation in domain (i):

$$\tilde{T}_i = \tilde{p}_i \tilde{v}_{g_i} = (\tilde{P}_i - \tilde{k}) \tilde{v}_{g_i} \quad \text{and} \quad \tilde{P}_i \approx 1. \quad (4.28)$$

Property:

Since $k > 0$ (see Appendix C), we must have $\tilde{T}_i/\tilde{v}_{g_i} < 1$. The limit case corresponds to:

$$\tilde{T}_i = \tilde{v}_{g_i}. \quad (4.29)$$

We hypothesize that the condition (4.29) defines the value of the Leidenfrost temperature. In the following we will show that this hypothesis fits with experimental observations.

5 Dimensionless equations of energy

5.1 Liquid–vapor interface (i)

The condition (3.18) across the liquid–vapor interface writes:

$$\frac{1}{2} q^2 v_{g_i}^2 + \mu(v_{g_i}, T_i) + k v_{g_i} = \frac{1}{2} q^2 v_{l_i}^2 + \mu(v_{l_i}, T_i),$$

and Eq. (2.2) yields:

$$\frac{1}{2} q^2 v_{g_i}^2 + k v_{g_i} - R T_i \left\{ \text{Log} \left(\frac{v_{g_i} - b}{v_{l_i} - b} \right) - b \left(\frac{1}{v_{g_i} - b} - \frac{1}{v_{l_i} - b} \right) \right\} + 2a \left(\frac{1}{v_{l_i}} - \frac{1}{v_{g_i}} \right) = 0.$$

As proved in Section 4 we can neglect \tilde{q}^2 and one obtains:

$$\tilde{k} \tilde{v}_{g_i} - \tilde{T}_i \left\{ \text{Log} \left(\frac{\tilde{v}_{g_i} - \tilde{b}}{\tilde{v}_{l_i} - \tilde{b}} \right) - \tilde{b} \left(\frac{1}{\tilde{v}_{g_i} - \tilde{b}} - \frac{1}{\tilde{v}_{l_i} - \tilde{b}} \right) \right\} + 2\tilde{a} \left(\frac{1}{\tilde{v}_{l_i}} - \frac{1}{\tilde{v}_{g_i}} \right) = 0. \quad (5.30)$$

5.2 Non-isothermal vapor-layer (b)

For the specific heat at constant pressure c_p , we choose a quadratic model in temperature (see Figure 2):

$$c_p(T) = H_1 + 2 H_2 T + 3 H_3 T^2. \quad (5.31)$$

By integration, we obtain:

$$\int_{T_w}^{T_i} c_p(T) dT = H_1 (T_i - T_w) + H_2 (T_i^2 - T_w^2) + H_3 (T_i^3 - T_w^3).$$

This is the custom to consider locally a linear approximation for $L(T)$ [35]:

$$L(T) = L_0 + L_1 T \quad \text{where} \quad L_1 < 0. \quad (5.32)$$

With (5.31) and (5.32), Eq. (3.25) becomes:

$$\begin{aligned} \frac{1}{2} q^2 (v_{g_i}^2 - v_w^2) + 2k v_{g_i} + H_1 (T_i - T_w) + H_2 (T_i^2 - T_w^2) + H_3 (T_i^3 - T_w^3) \\ + R (T_i - T_w) + L_1 (T_i - T_w) = 0. \end{aligned} \quad (5.33)$$

Neglecting terms associated with \tilde{q}^2 , dimensionless form of (5.33) writes:

$$\begin{aligned} 2\tilde{k} \tilde{v}_{g_i} + \tilde{H}_1 (\tilde{T}_i - \tilde{T}_w) + \tilde{H}_2 (\tilde{T}_i^2 - \tilde{T}_w^2) + \tilde{H}_3 (\tilde{T}_i^3 - \tilde{T}_w^3) \\ + (\tilde{T}_i - \tilde{T}_w) + \tilde{L}_1 (\tilde{T}_i - \tilde{T}_w) = 0, \end{aligned} \quad (5.34)$$

$$\text{where,} \quad \tilde{H}_1 = \frac{H_1}{R}, \quad \tilde{H}_2 = \frac{H_2 T_0}{R}, \quad \tilde{H}_3 = \frac{H_3 T_0^2}{R}, \quad \tilde{L}_1 = \frac{L_1}{R}.$$

5.3 Consequences

In dimensionless form, Eq. (4.26) writes:

$$(\tilde{v}_{i_i} - \tilde{b}) \tilde{v}_{i_i}^2 - \tilde{T}_i \tilde{v}_{i_i}^2 + (\tilde{v}_{i_i} - \tilde{b}) \tilde{a} = 0. \quad (5.35)$$

Using (4.28), one obtains:

$$\tilde{k} \tilde{v}_{g_i} = \tilde{v}_{g_i} - \tilde{T}_i. \quad (5.36)$$

Taking account of Eqs. (5.30), (5.34) and (5.35), and by using relation (5.36), the system allowing to solve our problem is:

$$\left\{ \begin{array}{l}
\tilde{v}_{g_i} - \tilde{T}_i - \tilde{T}_i \left\{ \text{Log} \left(\frac{\tilde{v}_{g_i} - \tilde{b}}{\tilde{v}_{l_i} - \tilde{b}} \right) - \tilde{b} \left(\frac{1}{\tilde{v}_{g_i} - \tilde{b}} - \frac{1}{\tilde{v}_{l_i} - \tilde{b}} \right) \right\} \\
+ 2 \tilde{a} \left(\frac{1}{\tilde{v}_{l_i}} - \frac{1}{\tilde{v}_{g_i}} \right) = 0, \\
2 \left(\tilde{v}_{g_i} - \tilde{T}_i \right) + \tilde{H}_1 \left(\tilde{T}_i - \tilde{T}_w \right) + \tilde{H}_2 \left(\tilde{T}_i^2 - \tilde{T}_w^2 \right) \\
+ \tilde{H}_3 \left(\tilde{T}_i^3 - \tilde{T}_w^3 \right) + \left(\tilde{T}_i - \tilde{T}_w \right) + \tilde{L}_1 \left(\tilde{T}_i - \tilde{T}_w \right) = 0, \\
\tilde{T}_i - \left(\tilde{v}_{l_i} - \tilde{b} \right) \left(\frac{\tilde{a}}{\tilde{v}_{l_i}^2} - 1 \right) = 0.
\end{array} \right. \quad (5.37)$$

System (5.37) is a system of three equations relatively to unknowns $\tilde{v}_{g_i}, \tilde{v}_{l_i}, \tilde{T}_i$.

6 Numerical study

6.1 Values of specific isobaric capacities of water vapor

The table, giving the values of specific isobaric capacities for water vapor, is taken from [19, 35].

$T^{\circ C}$	90 °C	100 °C	120 °C	140 °C	160 °C	180 °C	200 °C
$T^{\circ K}$	363 °K	373 °K	393 °K	413 °K	433 °K	453 °K	473 °K
c_p	2042.9	2080	2177	2310.9	2488.3	2712.9	2989.5

Table 1: Isobaric heat capacity of water vapor is expressed in $J kg^{-1} K^{-1}$. The different temperature values are given together in degrees Celsius and Kelvin.

The following quadratic relation is used linking the heat capacity at constant pressure (in $J kg^{-1} K^{-1}$) as a function of the temperature T expressed in degrees Kelvin:

$$c_p(T) = 8329 + 37.13 T - 0.05460 T^2. \quad (6.38)$$

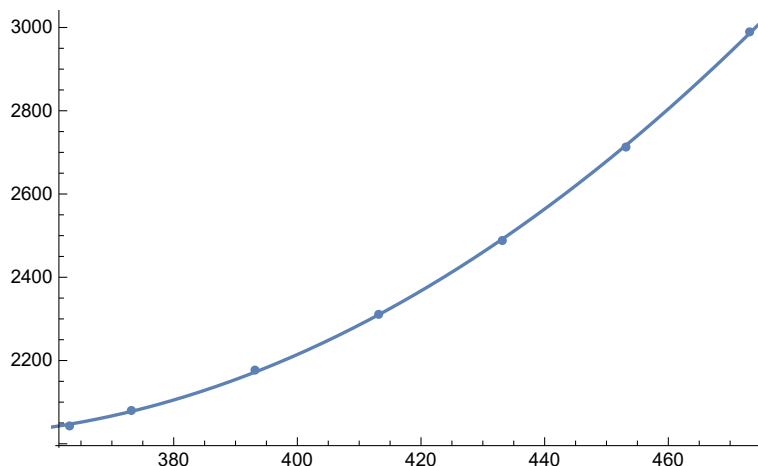


Figure 2: Graph associated with experimental Table 1 and Relation (6.38). The x -axis indicates the Kelvin temperature, and the y -axis indicates the corresponding isobaric heat capacity c_p expressed in $J\ kg^{-1}\ K^{-1}$. The dots represent c_p values coming from experimental Table 1.

Then

$$\int_{T_w}^{T_i} c_p(T) dT = H_1 (T_i - T_w) + H_2 (T_i^2 - T_w^2) + H_3 (T_i^3 - T_w^3),$$

with

$$H_1 = 8329, \quad H_2 = 18.56, \quad H_3 = -0.01820.$$

Here and in the following, we do not indicate SI – dimensions of H_i coefficients. The experimental values of c_p are given in Table 1. The corresponding approximation (6.38) is shown in Fig. 2. We see that Relation (6.38) fits perfectly with experiment values.

6.2 Values of latent heat of vaporization for water

The table giving the values of latent heat of vaporization for water as a function of temperature is taken from [19, 35]. Usually, a local linear approximation of the latent heat $L(T)$ in $kJ\ kg^{-1}$ (kilojoule per kilogram) is used as a function of temperature T expressed in degrees Kelvin. Below, we consider two very close approximations of $L(T)$ to understand how the results

$T\text{ }^{\circ}C$	90 °C	100 °C	110 °C	120 °C	130 °C	140 °C	150 °C	160 °C	170 °C	180 °C	190 °C	200 °C
$T\text{ }^{\circ}K$	363 °K	373 °K	383 °K	393 °K	403 °K	413 °K	423 °K	433 °K	443 °K	453 °K	463 °K	473 °K
L	2283.3	2256.4	2229.6	2202.1	2173.7	2144.3	2113.7	2082.0	2048.8	2014.2	1977.9	1939.7

Table 2: The latent heat of liquid water to be transformed into vapor is expressed in $kJ\text{ }kg^{-1}$. The different temperature values are given both in degrees Celsius and Kelvin.

obtained are sensible to experimental errors in measuring of the latent heats. Indeed, the data shown in Table 6.2 correspond to static measurements. In dynamics, the static latent heat is only a rough approximation: we do not take account of the heat radiation, physico-chemical state and geometry of the heating surface, non-equilibrium process of evaporation, etc.

- First linear approximation:

$$L(T) = 3295 - 2800 T \quad (6.39)$$

- Second linear approximation:

$$L(T) = 3385 - 2900 T \quad (6.40)$$

These two close approximations are shown in Fig. 3.

What matters is the difference of the latent heats $L(T_i)$ and $L(T_w)$. Hence, only the slope in T is relevant. As we will see, the variation of 3% of slopes between (6.39) and (6.40), implies a sensible variation of the Leidenfrost temperature.

6.3 Calculations of Leidenfrost's temperature

We solve the system (5.37) by using the software *Mathematica*TM. As a and b have a little variation with temperature, we take:

$$a \approx 1.488 \times 10^3\text{ }m^5\text{ }s^{-2} \quad \text{and} \quad b \approx 9.212 \times 10^{-4}\text{ }m^3\text{ }kg^{-1},$$

as intermediate values associated with (2.4) and (2.5). Thus, (4.27) yields:

$$\tilde{a} = 5.19685 \times 10^{-3} \quad \text{and} \quad \tilde{b} = 5.48001 \times 10^{-4}.$$

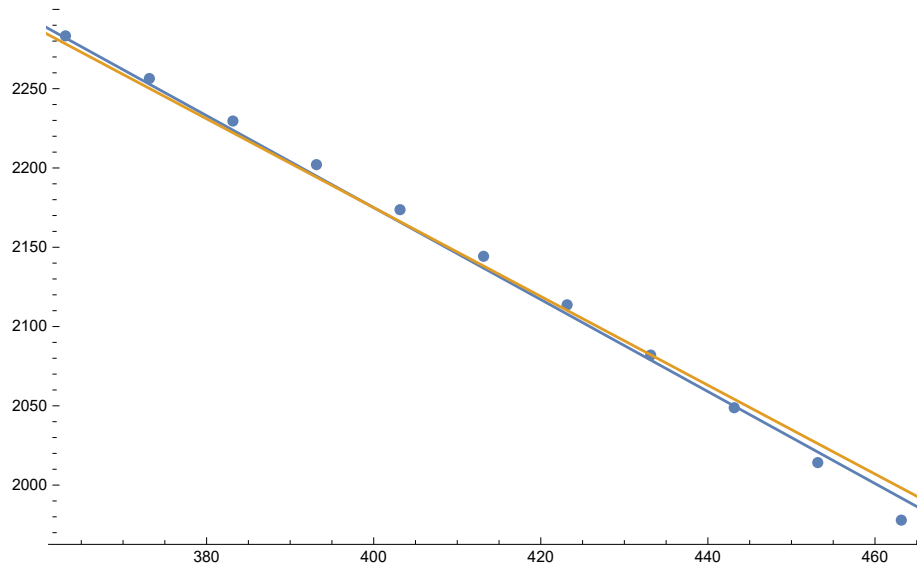


Figure 3: The linear approximations of the latent heat in $kJ\ kg^{-1}$ expressed by (6.39) (in yellow) and (6.40) (in blue) are shown as functions of the Kelvin temperature. The dots represent the values of $L(T)$ from Table 2.

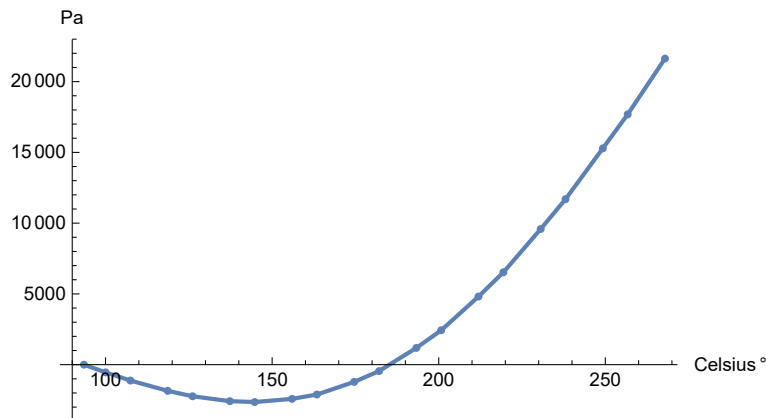


Figure 4: Graphs associated with the k values in the *first linear approximation* (6.39). The x -axis is associated with the Celsius temperature and the y -axis with the pressure k expressed in Pascal. The dots represented k values calculated with the software *Mathematica*TM.

$T_w \text{ } ^\circ C$	93.5 °C	100 °C	119 °	137 °C	156 °C	175 °C	193 °C	212 °C
\tilde{T}_w	0.983	1	1.05	1.10	1.15	1.20	1.25	1.30
\tilde{v}_{g_i}	0.983	0.977	0.965	0.958	0.960	0.971	0.994	1.032
\tilde{T}_i	0.983	0.983	0.983	0.983	0.983	0.983	0.983	0.983
\tilde{v}_{l_i}	0.000621	0.000621	0.000621	0.000621	0.000621	0.000621	0.000621	0.000621

Table 3: Calculations of \tilde{v}_{g_i} , \tilde{T}_i , \tilde{v}_{l_i} as a function of T_w by using the first linear approximation (6.39).

For the first linear approximation (6.39) the corresponding Table 3 is formed. The condition $\tilde{v}_{g_i} = \tilde{T}_i$ corresponds to the fact that k changes its sign. The value of T_w associated with bifurcation (4.29) is our definition of the Leidenfrost temperature which will be denoted by T_L . From the Table 3 one can see that $\tilde{T}_i > \tilde{v}_{g_i}$ at $\tilde{T}_w = 1.20$ but $\tilde{T}_i < \tilde{v}_{g_i}$ at $\tilde{T}_w = 1.25$. At $\tilde{T}_w = \tilde{T}_L \approx 1.23$ one has $\tilde{T}_w = \tilde{v}_{g_i}$. This critical value is the Leidenfrost temperature \tilde{T}_L . In this case, $T_L \approx 185^\circ C$.

For $T_w < T_L$ ($k < 0$) the liquid film sticks to the solid surface by causing the nucleate boiling. For $T_w > T_L$ ($k > 0$) the vapor film exists. In Fig. 4, we represent the value of k as a function of T_w in degrees Celsius.

$T_w \text{ } ^\circ C$	93.5 °C	100 °C	119 °	137 °C	156 °C	175 °C	193 °C	212 °C
\tilde{T}_w	0.983	1	1.05	1.10	1.15	1.20	1.25	1.30
\tilde{v}_{g_i}	0.983	0.975	0.958	0.946	0.941	0.947	965	997
\tilde{T}_i	0.983	0.983	0.983	0.983	0.983	0.983	0.983	0.983
\tilde{v}_{l_i}	0.000621	0.000621	0.000621	0.000621	0.000621	0.000621	0.000621	0.000621

Table 4: Calculations of \tilde{v}_{g_i} , \tilde{T}_i , \tilde{v}_{l_i} as a function of T_w by using the second linear approximation (6.40) .

For the second linear approximation (6.40) the corresponding Table 4 is formed. The results are similar but the associated temperature corresponds to $\tilde{T}_L \approx 1.28$ i.e. $T_L \approx 204^\circ C$. On Fig. 5, we represent the value of k as a function of T_w .

When \tilde{T}_i is eliminated from the third equation of (5.37), only two equations for v_{l_i} and v_{g_i} have to be solved. We show in Fig. 6 the intersection of the two corresponding curves for the the first linear approximation (6.39) and for the value of $\tilde{T}_w = 1.23$ corresponding to $T_w = 185^\circ$ Celsius. The intersection point is not sensitive to the choice of parameters \tilde{a} and \tilde{b} .

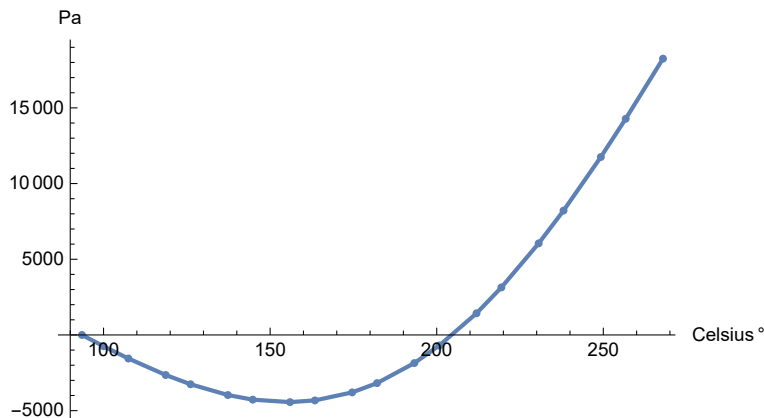


Figure 5: Graphs associated with the k values in the *second linear approximation* (6.40). The x -axis is associated with the Celsius temperature and the y -axis with the pressure k expressed in Pascal. The dots represented k values calculated with the software MathematicaTM.

In the literature, a wide range of values of Leidenfrost's temperature were measured depending on the surface characteristics [12]. It is the main reason we give *two close approximations* for the latent heat of vaporisation. These two approximations are very close but the two temperatures T_L are noticeably different. Such quite wide dispersion of values of the Leidenfrost temperature was experimentally observed [6, 11]. We recall that one of the possible reason of this dispersion is the surface physico-chemical characteristics. The temperature $T_L \approx 150^\circ$ Celsius corresponds to the lowest value obtained experimentally, but depending on the characteristics of the surface, the Leidenfrost temperature can be much higher than $T_L \approx 204^\circ$ Celsius [12].

Another important observation results in the computation of temperature T_i of the liquid bulk. The temperature of the liquid was first measured in the 19th century by Boutigny [11] who discovered that temperature T_i is lower than 100° Celsius. Precise measurements give the temperature of liquid bulk between 92° and 94° Celsius [36]. In our model, the temperature of interface is $T_i \approx 93.5^\circ$ Celsius corresponding to $\tilde{T}_i \approx 0.983$. For both approximations (6.39) and (6.40) the T_i values are the same. This result is another confirmation of the consistency of our model.

Based on the variation of k one can simply explain the Leidenfrost phenomenon as follows. If $k > 0$, the thermodynamic pressure p is lower in the

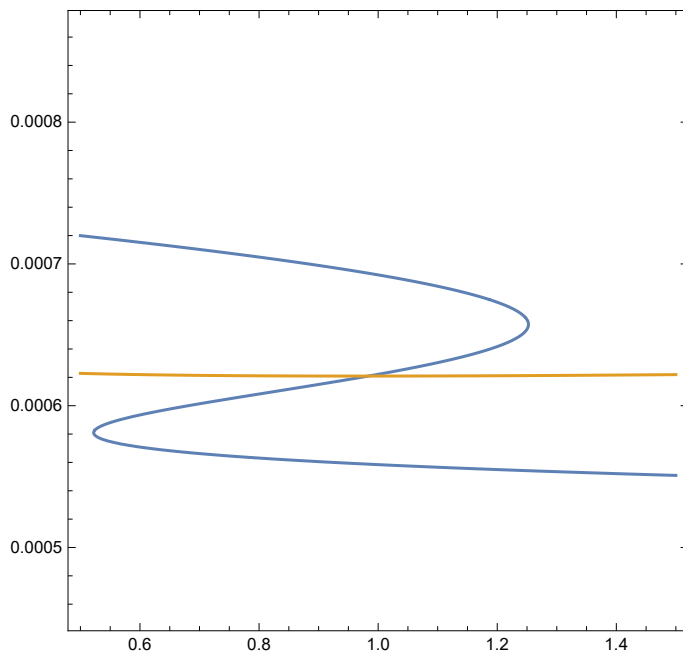


Figure 6: Contour-graphs associated with the two first equations of system (5.37) are shown in the case $\tilde{T}_w = 1.23$, when \tilde{T}_i is eliminated from the third equation. The Z - *shape* curve corresponds to the equation (5.37)₂, the second curve corresponds to (5.37)₁. The horizontal (vertical) axis indicates dimensionless vapor and liquid specific volumes, respectively. The curves intersect transversally in a unique point. These graphs prove that solution is little sensitive to the approximation of physical parameters.

vapor phase just near the liquid-vapor interface compared to the pressure p_0 near the surface. This results to a detachment of the liquid film from the surface. On the contrary, if $k < 0$, the thermodynamic pressure p is higher, and liquid film wets the surface causing a violent boiling. In fact the whole process is highly non-stationary and cannot be described by the stationary equations. However, our approach gives a reasonable estimation of the Leidenfrost temperature.

7 Conclusion

We study the film boiling phenomenon in the framework of the internal capillarity model. The capillary pressure term k allows us to understand the phenomenon and to determine the Leidenfrost temperature. The boiling crisis corresponds to $k > 0$, and Leidenfrost's temperature to $k = 0$. The model predicts the Leidenfrost temperature which fits with experimental results. A second important result is the estimation of the temperature of the liquid bulk. It is proved that its value is below the boiling temperature at atmospheric pressure. This result is also compatible with the experimental data on the liquid bulk temperature.

Acknowledgments: The authors thank D. Brutin and B. Darbois-Textier for pointing out to us useful references. The authors are partially supported by Agence Nationale de la Recherche, France (SNIP ANR-19-ASTR-0016-01).

References

- [1] J. Walker, *The amateur scientist*. Scientific American, **237**, 126-131 (1977).
- [2] F. Celestini, T. Frisch, Y. Pomeau, *Take-off of small Leidenfrost droplets*, Phys. Rev. Lett., **109**, 034501 (2012).
- [3] D. Quéré, *Leidenfrost dynamics*, Annu. Rev. Fluid. Mech., **45**, 197-215 (2013).

- [4] B. Darbois-Textier, G. Dupeux, G. Lagubeau, M. Le Merrer, K. Piroird, D. Soto, C. Clanet, D. Quéré, *La Caléfaction*. *Reflète phys.*, **37**, 12–16 (2013).
- [5] Y. Pomeau, M. Le Berre, F. Celestini, T. Frisch, *The Leidenfrost effect: From quasi-spherical droplets to puddles*, *C. R. Mec.*, **340**, 867–881 (2012).
- [6] A.L. Biance, C. Clanet, D. Quéré, *Leidenfrost drops*, *Physics of Fluids*, **15**, 1632 (2003).
- [7] N. J. Holter, W. R. Glasscock, *Vibrations of evaporating liquid drops*, *The Journal of the Acoustical Society of America*, **24**, 6, 682–686 (1952).
- [8] X. Ma, J.-J. Liéter-Santos, J.C. Burton, *Star-shaped oscillations of Leidenfrost drops*, *Phys. Rev. Fluids*, **2**, 031602 (2017).
- [9] P. Casal, H. Gouin, *Vibrations of liquid drops in film boiling phenomena*, *Int. J. Engineering Science*, **32**, 10, 1553–1560 (1994).
- [10] J. G. Leidenfrost. *De aquae communis nonnullis qualitatibus tractatus*, Duisburg (1756); translated by C. Wares, *On the fixation of water in diverse fire*, *Int. J. Heat Mass Transfer*, **9**, 1153–1166 (1966).
- [11] M. Boutigny. *Sur les phénomènes que présentent les corps projetés sur des surfaces chaudes*, *Annales de Chimie et Physique*, **3**, IX 350–370 (1843) and **3**, XI, 16–39 (1844).
- [12] J. D. Bernardin, I. Mudawar, *The Leidenfrost point: Experimental study and assessment of existing models*, *J. Heat Transfer*, **121**, 894–903 (1999).
- [13] P. Sadasivan, C. Unal, R. Nelson, *The need for new experiments*, *J. Heat Transfer*, **117**, 558–567 (1995).
- [14] P. Sadasivan, C. Unal, R. Nelson, *Nonlinear aspects of high heat flux nucleate boiling heat transfer*, *J. Heat Transfer*, **117**, 981–989 (1995).
- [15] J.M. Delhaye, M. Giot, M.L. Riethmuller (eds). *Thermohydraulics of two-phase systems for industrial design and nuclear engineering*. Mc Graw-Hill, New York (1981).

- [16] V. S. Nikolayev, D. Chatain, Y. Garrabos, D. Beysens, *Experimental evidence of the vapor recoil mechanism in the boiling crisis*, Phys. Rev. Lett., **97**, 184503 (2006).
- [17] P. Lloveras, F. Salvat-Pujol, L. Truskinovsky, E. Vives, *Boiling Crisis as a Critical Phenomenon*, Phys. Rev. Lett., **108**, 215701 (2012).
- [18] F. Celestini, T. Frisch, A. Cohen, C. Raufaste, L. Duchemin, Y. Pomeau, *Two dimensional Leidenfrost droplets in a Hele-Shaw cell*, Physics of Fluids, **26**, 032103 (2014).
- [19] J. Rumble (Ed.) *Handbook of Chemistry and Physics 102nd Edition*. CRC Press, Boca Raton, Floride, USA (2021).
- [20] P. Germain, *The method of virtual power in the mechanics of continuous media, I: Second-gradient theory*, Mathematics and Mechanics of Complex Systems, **8**, No. 2, 153–190 (2020). Translated by Marcelo Epstein and Ronald E. Smelser from P. Germain, *La méthode des puissances virtuelles en mécanique des milieux continus, I. La théorie du second gradient*, J. de Mécanique, 12, 235–274 (1973).
- [21] P. Casal, *La théorie du second gradient et la capillarité*, C.R. Acad. Sci. Paris, **274 A** 1571–1574 (1972).
- [22] J.S. Rowlinson, B. Widom, *Molecular Theory of Capillarity*. Clarendon Press, Oxford (1984) and books.google.com (2013).
- [23] P. Casal, *Principes variationnels en fluide compressible et en magnétodynamique des fluides*, J. de Mécanique, **5**, n^o 2, 149–161 (1966).
- [24] H. Gouin, *Utilization of the second gradient theory in continuum mechanics to study the motions and thermodynamics of liquid-vapor interfaces*, Physicochemical Hydrodynamics, Serie B: Physics, **174**, 666–682 (1987).
- [25] S.L. Gavriluk, H. Gouin, *Rankine–Hugoniot conditions for fluids whose energy depends on space and time derivatives of density*, Wave Motion, **98**, 102620 (2020).
- [26] H. Gouin, *Rankine–Hugoniot conditions obtained by using the space – time Hamilton action*, Ricerche di Matematica, 70, 115–129 (2021).

- [27] P. Casal, H. Gouin, *Connection between the energy equation and the motion equation in Korteweg's theory of capillarity*, C.R. Acad. Sci. Paris, **300** (II) 231–234 (1985).
- [28] S. Gavriluk, B. Nkonga, K-M. Shyue, L. Truskinovsky, *Stationary shock-like transition fronts in dispersive systems*, Nonlinearity, **33** 547–509 (2020).
- [29] S. Gavriluk, K-M. Shyue, *Singular solutions of the BBM equation: analytical and numerical study*, Nonlinearity **35**, 388–410 (2022).
- [30] H. Gouin, W. Kosiński, *Boundary conditions for a capillary fluid in contact with a wall*, Arch. Mech., **50**, 907–916 (1998).
- [31] B. V. Derjaguin, N. V. Churaev, V. M. Muller, *Surfaces Forces*. Springer, New-York (1987).
- [32] H. Gouin, *Liquid nanofilms. A mechanical model for the disjoining pressure*, Int. J. Engineering Science, **47**, 691-699 (2009).
- [33] Y. Rocard, *Thermodynamique*. Masson, Paris (1967).
- [34] A-L. Himbert-Biance, *Gouttes inertielles: de la caléfaction à l'étalement*. PhD thesis, Sorbone University, 11 July 2005.
- [35] E.W. Lemmon, M.L. Hubert, M.O. McLinden, NIST Standard Reference Database 23: Reference *Fluid Thermodynamic and Transport Properties*-REFPROP Version 9.0, National Institute of Standards and technology, Standard Reference Data Program, Gaithersburg, Maryland, 2010. (www.nist.gov/srd/nist23.cfm)
- [36] N. Tokugawa, R. Takaki. *Mechanism of self-induced vibration of a liquid drop based on the surface tension fluctuation*, J. Phys. Soc. Jpn., **63**, 1758–1768, (1994).

A Extra-condition at dynamical liquid-vapor interfaces

Extra-condition (3.21) does not come from conservation laws. It is a natural boundary condition coming from Lagrangian formulation of the problem. It

already appeared in the study of discontinuous solutions of dispersive equations [25, 28, 29]. To give a proof in one-dimensional case, we consider a general action functional:

$$a\{y\} = \int_I \mathcal{L}(y, y') dx,$$

$y(x)$ is an unknown function, and the integral is taken over a finite interval I . The values of $y(x)$ are fixed at the ends of interval I . We are looking for $y(x)$ on which the functional is extremal and we do not assume that $y(x)$ is smooth. The variation of a can be written as:

$$\delta a = \int_I \left\{ \frac{\delta \mathcal{L}}{\delta y} \delta y + \frac{d}{dx} \left(\frac{\partial \mathcal{L}}{\partial y'} \delta y \right) \right\} dx, \quad \text{with} \quad \frac{\delta \mathcal{L}}{\delta y} = \frac{\partial \mathcal{L}}{\partial y} - \frac{d}{dx} \left(\frac{\partial \mathcal{L}}{\partial y'} \right).$$

In the case of non-smooth (or "broken") extremal curves, the same Euler–Lagrange equation should be satisfied for each smooth part of the extremal curve:

$$\frac{\delta \mathcal{L}}{\delta y} = 0. \tag{A.41}$$

Together with (A.41) an additional condition should also be satisfied at the "broken" point:

$$\left[\frac{\partial \mathcal{L}}{\partial y'} \right] = 0. \tag{A.42}$$

In the case of capillary fluids, \mathcal{L} is quadratic with respect to y' because λ is constant. It implies that y' is continuous at the *broken* point. Condition (A.42) is usually called *Weierstrass-Erdmann* condition, or *corner* condition. In particular, if a piecewise C^2 -solution $y(x)$ is constant on some interval of x , but is not constant on a neighboring interval, this solution should have a zero slope at the broken point.

B Special cases of capillary fluid motions

B.1 Isothermal motions

In the case of isothermal stationary motion, the whole entropy of domain \mathcal{D}_t corresponding to the bulk (a) and interface (i) is:

$$\int_{\mathcal{D}_t} \rho \eta dD = S_0, \tag{B.43}$$

where S_0 is constant (independent of time t), and dD is the elementary volume. Due to constraint (B.43), Hamilton's action is modified into: there exists a constant Lagrange multiplier T_0 such that the new Lagrangian \mathcal{L} is associated with $\alpha - T_0 \eta$ which is the specific free energy at constant temperature. The application of the Hamilton principle yields the same equations of motion where α has to be replaced by $\alpha - T_0 \eta$. Consequently, the specific enthalpy is replaced by the chemical potential μ . The variation of η implies $T - T_0 = 0$.

B.2 Motions at constant pressure

In the case of stationary motions, if domain \mathcal{D}_t is an invariant control volume through which the steam flows, it verifies:

$$\int_{\mathcal{D}_t} dD = \mathcal{V}_0, \quad (\text{B.44})$$

where \mathcal{V}_0 is constant (independent of time t). Due to constraint (B.44), Hamilton's action is modified into: there exists a constant Lagrange multiplier p_0 such that the new Lagrangian \mathcal{L} is associated with $H = \alpha + p_0/\rho$, which is the specific enthalpy at constant pressure p_0 . Consequently, in Subsection 3.1, in the energy equation, the specific energy should be replaced by the specific enthalpy at constant pressure p_0 , and the equation of motion is unchanged.

C Isothermic oscillations of the vapor density near liquid-vapor interface (i)

We look for oscillating stationary vapor flow in the immediate vicinity of interface (i) where the temperature is T_i . The governing equation of motions in the vapor phase is deduced from Eqs (3.13)–(3.14), and writes in the form:

$$\lambda \frac{d^2 \rho}{dx^2} = \mu(\rho, T_i) + \frac{q^2}{2\rho^2} + r, \quad \text{where } r = \text{const.}$$

The vapor is considered as an ideal gas; we get the potential μ , defined up to an additive constant which can be included in r :

$$\mu(\rho, T_i) = c_{T_i}^2 \text{Log } \rho, \quad \text{where } c_{T_i}^2 = RT_i.$$

Here c_{T_i} denotes the isothermal sound velocity of vapor at temperature T_i . To obtain oscillatory solutions, we choose a special value of r replacing it by a new constant ρ_{**} :

$$\lambda \frac{d^2 \rho}{dx^2} = c_{T_i}^2 \text{Log} \left(\frac{\rho}{\rho_{**}} \right) + \frac{q^2}{2\rho^2} - \frac{q^2}{2\rho_{**}^2}. \quad (\text{C.45})$$

Integrating Eq. (C.45), one obtains:

$$\frac{\lambda}{2} \left(\frac{d\rho}{dx} \right)^2 = F(\rho) - d, \quad \text{where } d = \text{const}. \quad (\text{C.46})$$

with

$$F(\rho) = c_{T_i}^2 \left(\rho \text{Log} \left(\frac{\rho}{\rho_{**}} \right) - \rho + \rho_{**} \right) - \frac{q^2}{2\rho} \left(1 - \frac{\rho}{\rho_{**}} \right)^2.$$

By construction,

$$F(\rho_{**}) = 0, \quad \frac{dF}{d\rho}(\rho_{**}) = 0.$$

The variation of F for $M_i^2 = q^2/(\rho_{g_i} c_{T_i})^2 < 1$ is shown in Figure 7 ⁽¹⁾. It has a unique maximum point ρ_* such that $0 < \rho_* < \rho_{**}$. Moreover, $F \rightarrow -\infty$ as $\rho \rightarrow +0$. Hence, for any d such that $0 < d < F(\rho_*)$ one has a solution of (C.46) oscillating between ρ_{imin} and ρ_{imax} , where $F(\rho_{imin}) = F(\rho_{imax}) = d$ (see Figure 7). The solution of (C.46) is schematically shown in Figure 8 (on the left). The liquid–vapor interface is considered as a discontinuity. So, the density jumps from ρ_l to the extreme value of the vapor density (see the extra condition (3.21)). Since we have two possible values (minimum and maximum values), the choice has to be done. Obviously, the jump from ρ_l to ρ_{imax} has a smaller amplitude compared to that from ρ_l to ρ_{imin} , and hence the smallest energy variation. Also, physically, only this choice allows us to obtain ‘levitation’ of the liquid film. Such a stationary periodic solution gives us just an idea about a strong density variation near the interface. Indeed, due to the boundedness of vapor region and the fact that a real flow is multi-dimensional, the vapor region represents rather a transition zone from oscillatory regime to a constant solution near the surface (see the right figure in Figure 8). However, this schematic picture does not influence the choice of the jump relations.

¹In liquid water $\rho_l \simeq 10^3 \text{kg/m}^3$. If boiling–evaporation time of a liquid film with 10^{-2} m thickness is about 100 s; then $u \simeq 10^{-4} \text{m/s}$ and for the liquid, the flow rate $q \simeq 10^{-1} \text{kg/m}^2 \cdot \text{s}$. In the vapor $\rho_l \simeq 1 \text{kg/m}^3$ and consequently $u \simeq 10^{-1} \text{m/s}$, and $M^2 \simeq 10^{-7} < 1$.

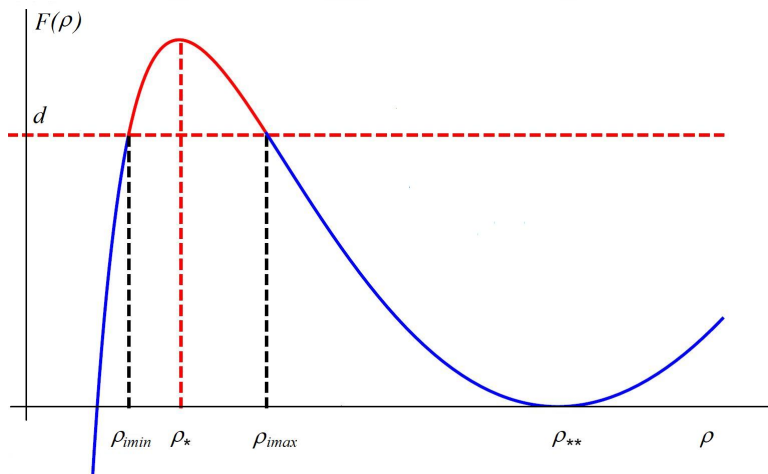


Figure 7: If $M_i^2 < 1$, the curve $F(\rho)$ has a local maximum at $\rho_* \in]\rho_{imin}, \rho_{imax}[$, and a local minimum at $\rho_{**} \in]\rho_{imax}, +\infty[$. We recall that $\rho = \rho_{**}$ is a formal value of ρ and that the physical part of the curve is only the *red part* of $F(\rho)$ corresponding to oscillations of density between ρ_{imin} and ρ_{imax} .

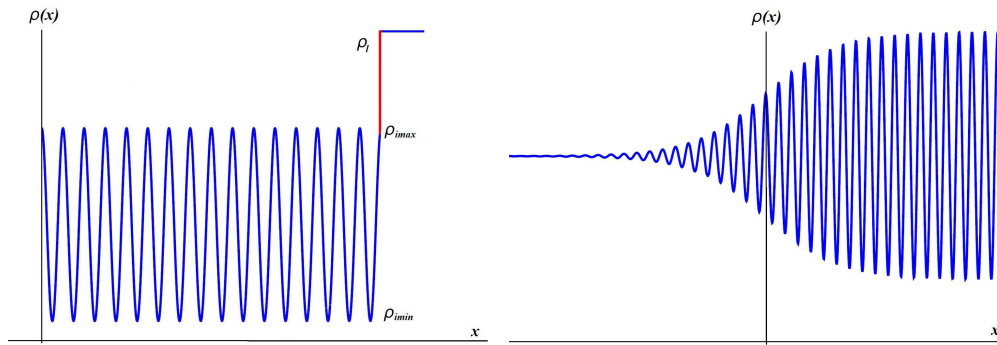


Figure 8: Left figure : The vapor density oscillates near the isothermal liquid-vapor interface. At the interface the density jumps (and decreases) from $\rho_{l_i} = 1/v_{l_i}$ to $\rho_{v_i} = 1/v_{g_i}$. The vapor density ρ_{v_i} being oscillating between two extrema ρ_{imin} and ρ_{imax} where $d\rho/dx = 0$, so we have to choose between these two values. The jump from ρ_{l_i} to ρ_{imax} has a smaller amplitude compared to that from ρ_{l_i} to ρ_{imin} , and hence a smaller energy decrease. Consequently, $d^2\rho/dx^2 < 0$ when $\rho_{v_i} = \rho_{imax}$ and $k = -\lambda \rho d^2\rho/dx^2 > 0$. Right figure : case of dissipative vapor flow. The oscillations of vapor density vanish near the surface boundary layer.